Optimization of Selective Oxidation for 850 nm (IR) and 780 nm (Far-red) Energy/Data Efficient Oxide-Confined Microcavity VCSELs

Michael Liu, Mong-Kai Wu, and Milton Feng

Department of Electrical and Computer Engineering · University of Illinois at Urbana-Champaign

Micro and Nanotechnology Laboratory · 208 N. Wright Street, Urbana, IL 61801

Phone: (217) 244-3662, e-mail: meliu2@illinois.edu

Keywords: Oxidation, Oxide Aperture, Vertical Cavity Surface-Emitting Laser (VCSEL)

Abstract

We compare the threshold current distribution of the VCSELs from two lots, 850 nm and 780 nm VCSELs, to examine the uniformity of the oxide aperture dimensions of the devices on the wafers. For the lot, the 850 nm VCSEL, with poor control in the oxidation process, the VCSELs show an average threshold current of 0.83 mA and a standard deviation of 0.089 mA. On the other hand, the other set of devices, the 780 nm VCSELs, which were fabricated with well-controlled oxidation show an average threshold current of 0.7 mA with a standard deviation of 0.032 mA. For microcavity VCSELs, the inability to achieve uniform oxidation will lead to device characteristics and performance inconsistency as well as low yield.

INTRODUCTION

With the burgeoning demand of high speed and energy efficient data transmission in the data centers, optical interconnect systems are being developed. Optical transceivers based on vertical-cavity surface-emitting lasers (VCSELs) have gained broad interests in high speed and low noise optical transceivers because of low threshold and high modulation bandwidth capability. Native oxide was a key invention that facilitated the development of the high speed and low threshold VCSELs [1-4]. By lateral oxidation, a high aluminum content AlGaAs layer oxidizes and forms an oxide aperture which can not only provide current confinement but also optical mode confinement through a refractive index contrast. The aperture size of a VCSEL is controlled by the wet oxidation, and thus the oxidation rate and uniformity then become the keys to obtain consistent aperture size in a batch. Microcavity VCSELs demonstrated higher bandwidth via Purcell enhancement while reducing power consumption [5]. These advantages make microcavity VCSELs extremely useful in short-hub interconnect systems. Recently, a microcavity VCSEL with an aperture dimension ~4 μm at 850 nm emission passed 40 Gb/s bit-error-rate test with an Energy/Data Efficiency of 430 fJ/bit

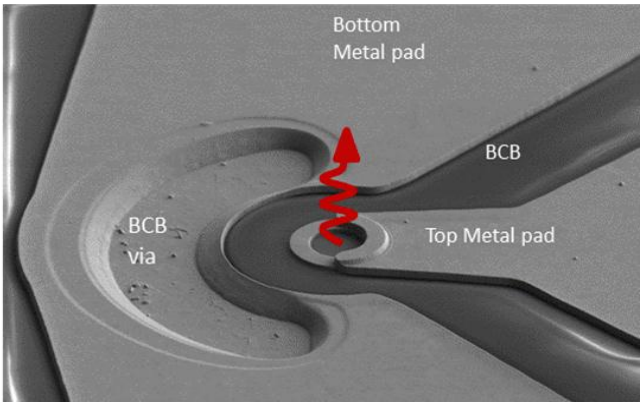

Figure 1. SEM image of the top view of a microcavity VCSEL

and relative intensity noise reaching the quantum limit [6-7]. Also, a 780 nm oxide-confined VCSEL with 13.5 Gb/s effort-free transmission was also demonstrated [8].

In this paper, we address the oxidation uniformity issue and the possible solution by comparing the distribution of the threshold current of the VCSELs from 2 different fabrication lots, 850 nm and 780 nm VCSELs. For the lot with poor control during the oxidation process, the devices' threshold current varies over a wide range. In a VCSEL, the threshold current is related to the volume of the active region which is directly related to the oxide aperture dimension. Thus, non-uniformity in the oxide aperture can be identified from variation in threshold current.

DEVICE FABRICATION

The epitaxial structure of the 850 nm VCSEL starts with 40 pairs of n-doped $Al_{0.15}Ga_{0.85}As/Al_{0.9}Ga_{0.1}As$ bottom DBR mirror, followed by the active region with 3 $In_{0.1}Ga_{0.9}As$ quantum wells, and another 22 pairs of p-doped $Al_{0.15}Ga_{0.85}As/Al_{0.9}Ga_{0.1}As$ top DBR including an $Al_{0.97}Ga_{0.03}As$ layer which can be oxidized as aluminum oxide for both electrical and optical confinement. The fabrication process starts with p-type Ti/Pt/Au metal contact evaporation, and then SiNx is deposited by PECVD and patterned with photoresist lithography and CF_4 dry etch as the hard mask. The top DBR mirror mesa

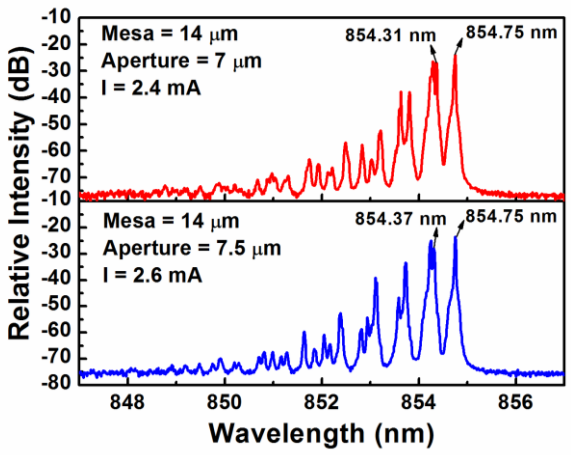

Figure 2. The emission spectra of two 850 nm VCSELs of oxide aperture diameters of 7 and 7.5 μm.

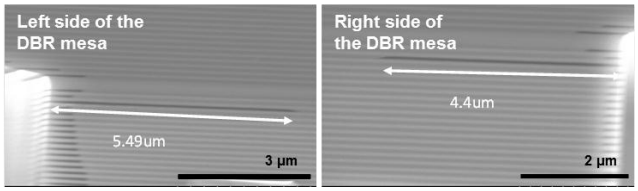

Figure 3. The cross section of a DBR mesa after oxidation in the unstable furnace for 7 minutes.

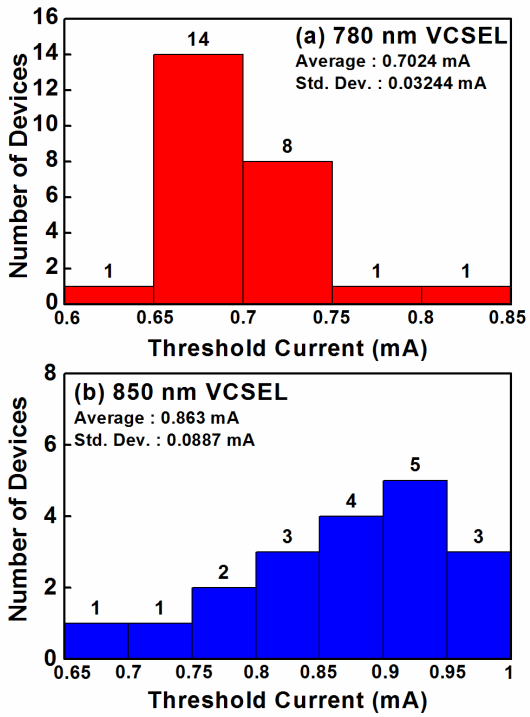

Figure 4. The threshold current distribution of the 2 VCSEL lots, 850 nm and 780 nm VCSELs. The 850 nm VCSELs are fabricated with an unstable furnace in the oxidation step.

is then created by inductively coupled plasma (ICP) RIE. After the dry etching, the sample is transferred to an oxidation furnace at 425 ºC filled with N_2 and H_2O vapor mixed gas to form an aluminum oxide aperture. Then, the bottom n-type contact AuGe/Ni/Au is evaporated and alloyed. The sample is planarized with BCB. After via opening, 1 μm Ti/Au metal interconnect is evaporated, and the device fabrication is finished. Figure 1 shows a SEM image of the finished device.

The main challenge of fabricating the microcavity VCSELs is to precisely control the aperture dimension. Figure 2 shows the measured spectra of two 850 nm VCSELs on the same wafer both biased at $I/I_{TH} = 3$. The variation in oxidation transfers to the laser spectrum profile. By estimating the mode spacing, the two devices are characterized to have oxide aperture diameters of 7 and 7.5 μm. When further reducing the oxide aperture diameter to below 3 μm, the inability to control the oxidation process will not only lead to device characteristics and performance variation on the wafer but also cause issues in yield. For microcavity VCSELs, a 0.5 μm difference may cause the threshold and mode spacing to vary more drastically than comparing 7 to 7.5 μm devices.

To have uniform oxidation for the aperture, the key is to have a well-controlled oxidation process. Our oxidation is conducted in an open-tube system with a quartz tube and an end cap seal. A push rod is secured in an orifice at the center of the end cap for loading the sample. The furnace temperature profile is measured with the thermal coupled probe, and the quartz boat for carrying the wafer is loaded to the hot zone of the furnace. Wet oxidation at lower temperatures leads to formation of aluminum hydroxide instead of aluminum oxide. Aluminum hydroxide is chemically unstable and may cause device reliability issues. The water vapor in our wet furnace is from a bubbler wrapped with heat tape and filled with DI water. We allow at least 3 hours for gas flow to stabilize in the furnace before the device oxidation process. The N_2 / H_2O mixing gas will escape from the furnace when opening the cap to load the sample. The sample loading time is then becoming a critical issue for having uniform oxidation in a batch. Typically, the sample loading should not be more than 20 seconds. After the wet oxidation, the sample will be moved into a dry N_2 furnace set at 410 ºC to drive out the moisture in the oxide layer. Figure 3 shows the SEM cross-section of a DBR mesa under wet oxidation for 7 minutes. It shows that even on a single mesa, the oxidation rate on different sides can vary. This issue is identified as unstable gas flow in the wet oxidation furnace due to excessive loading time. The longer the loading time, the more unpredictable the oxidation becomes. Figure 4 shows the threshold current of the devices for 2 VCSEL lots fabricated with the same process flow but different wet oxidation loading time. In the 780 nm VCSEL process, the loading time for the oxidation was controlled to around 20 seconds; however, in the 850 nm VCSEL process, the

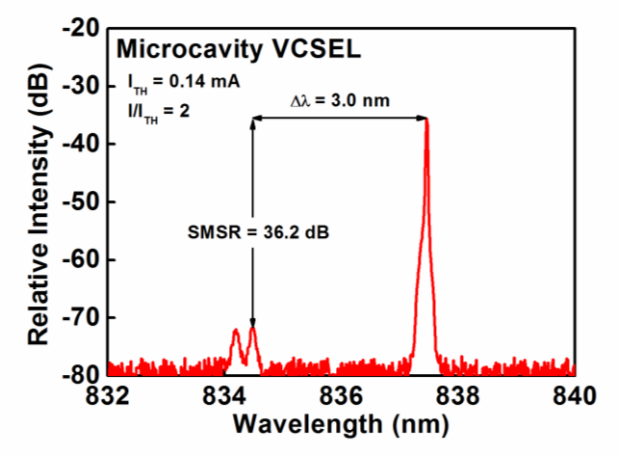

Figure 5. The spectrum of the 2 μm microcavity VCSEL with threshold current I_{TH} = 0.14 mA biased at 0.28 mA. The microcavity allows less high order modes in the gain profile.

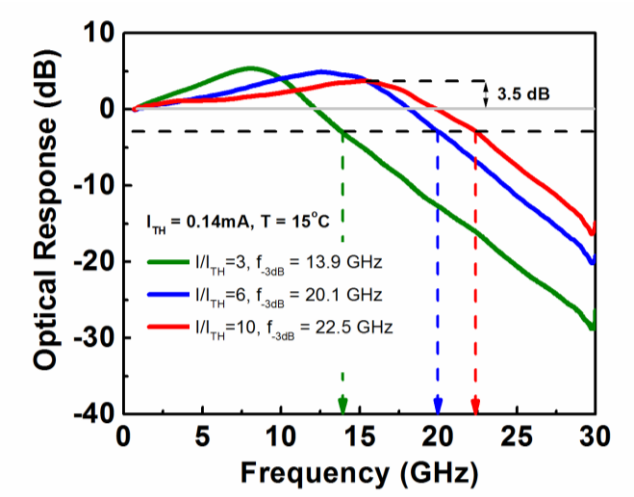

Figure 6. Optical response of the 2 μm microcavity VCSEL biased at I/I_{TH} = 3, 6, and 10. At I/I_{TH} = 10, the device shows a 3.5 dB resonance bump.

loading time was over 30 seconds. The 850nm VCSELs show variation from 0.66 to 0.98 mA for the threshold current with a standard deviation of 0.0887 mA. On the other hand, for most of the 780 nm VCSELs, their threshold current is in the range of 0.65-0.75 mA with a standard deviation of 0.032 mA. The threshold current is proportional to the volume of the active region in a VCSEL, and the lateral dimensions of the active region are controlled by the oxide aperture. From the data in Figure 4, oxidation process control plays an important role in the uniformity of device characteristics.

DEVICE CHARACTERIZATION AND RESULTS

To fabricate microcavity VCSELs with 2 μm oxide apertures, the oxidation rate needs to be carefully calibrated before the oxidation for the actual devices because for such dimensions fail to estimate the oxidation rate correctly may cause problems in yield. Figure 5 shows the emission spectrum of a 2 μm diameter microcavity VCSEL biased at I/I_{TH} = 2. It shows a mode spacing of 3 nm and a side mode suppression ratio (SMSR) of 36.2 dB, which is considered as single mode operation. Compared to the spectra of 7 and 7.5 μm VCSELs in Figure 2, the 2 μm cavity allows less optical modes to from standing-wave pattern within the cavity, so the generated photons from stimulated emission mainly contribute to the fundamental mode. Thus, the device exhibits a larger mode spacing and a larger SMSR.

To measure the optical microwave response of the device, the electrical microwave input signal is generated from port 1 of an Agilent Parametric Network Analyzer (PNA) and combined with the DC bias in a bias tee then sent into the microcavity VCSEL through GSG probes. The optical output is coupled into an optical fiber and converted to electrical signal by a photodector. Then, the converted signal is sent to port 2 of the PNA for

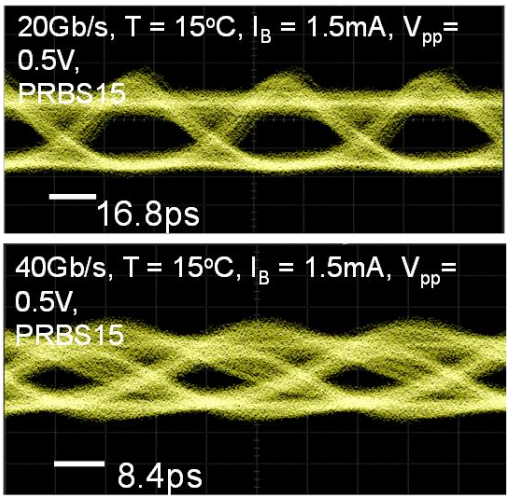

Figure 7. Eye diagrams at 20 Gb/s an 40 Gb/s data rates for the 2 μm microcavity VCSEL.

microwave response measurement. Figure 6 shows the optical frequency response of the 2 μm microcavity laser under I/I_{TH} = 3, 6, and 10, respectively. The modulation bandwidth increases from 13.9 to 22.5 GHz. The optical response does not show large resonant bump which indicates the recombination rate is enhanced by Purcell effect in the microcavity. A resonance bump will affect the signal integrity when the device is under modulation, and the distorted waveform will further lead to a "closed" eye diagram and thus limit the data transmission rate. An Agilent 81250 ParBERT signal generator is used to generate the 20 and 40 Gb/s NRZ 2^{15}–1 bit length pseudorandom binary series pattern with V_{pp} = 0.5 V AC voltage swing, and the eye diagram is captured by an Agilent 861000C oscilloscope. Figure 7 shows the eye

diagram at 20 Gb/s and 40 Gb/s of the 2 μm aperture microcvavity VCSEL biased at 1.5 mA at 15 ºC. The microcavity laser shows an open eye at 20 and 40 Gb/s data rates. The data/energy efficiency of the microcavity VCSEL is determined as 11.29 Gb/s/mW. However, due to insufficient optical output intensity, the device cannot pass the BER.

CONCLUSION

The non-uniformity of the oxide aperture dimensions in the microcavity VCSELs can be identified from the wide variation in the threshold current of the devices on the same wafer. While performing the aperture oxidation, the wafer needs to be placed in the hot zone of the furnace and the loading time needs to be short to minimize the instability of the gas flow in the furnace. For microcavity VCSELs with aperture dimensions around 2 μm, the calibration and control in the oxidation are critical for high yield. A microcavity can enhance the spontaneous recombination rate through Purcell effect and reduce the resonance bump in the optical microwave response of the VCSELs and lead to better signal integrity and higher modulation bandwidth.

ACKNOWLEDGEMENTS

The authors would like to thank prof. Nick. Holonyak, Jr. for the discussion and advices. The authors would also like to thank Dr. Michael Gerhold, Army Research Office, Land Mark Optoelectronic Corporation in Taiwan for 850 nm VCSEL material, Dr. Henry Pao for Yunni Pao and Family Fellowship, and MNTL Research Engineer Dr. Edmond Chow and Yaguang Lian for help with SEM and cleanroom equipment.

REFERENCES

[1] J. M. Dallesasse, N. Holonyak, A. R. Sugg, T. A. Richard, and N. El-Zein, "Hydrolyzation oxidation of Alx Ga1−x As-AlAs-GaAs quantum well heterostructures and superlattices," *Appl. Phys. Lett.*,vol. 57, no. 26, pp. 2844–2846, Oct. 1990.

[2] C. C. Hansing, H. Deng, D. L. Huffaker, D. G. Deppe, B. G. Streetman, and J. Sarathy, "Low-threshold continuous-wave surface emitting lasers with etched void confinement," *IEEE Photon. Technol. Lett.*, vol. 6, no. 3, pp. 320–322, Mar. 1994.

[3] D. L. Huffaker, D. G. Deppe, K. Kumar, and T. J. Rogers, "Native-oxide defined ring contact for low threshold vertical-cavity lasers," *Appl. Phys. Lett.*, vol. 65, no. 1, pp. 97–99, Jul. 1994.

[4] J. M. Dallesasse and N. Holonyak, "Oxidation of Al-bearing III–V materials: A review of key progress," *J. Appl. Phys.*, vol. 113, no. 5, pp. 051101-1–051101-11, Feb. 2013.

[5] F. Tan, C.H. Wu, M. Feng, and N. Holonyak, Jr., "Energy efficient microcavity lasers with 20 and 40Gb/s data transmission," *Appl. Phys. Lett.* vol. 98, no. 19, pp. 191107-1-191107-3, May 2011.

[6] F. Tan, M. K. Wu, M. Liu, M. Feng, and N. Holonyak, "850 nm oxide-confined VCSEL with low relative intensity noise and 40 Gb/s error free data transmission," *IEEE Photon. Technol. Lett.*, vol. 26, no. 3, pp. 289–292, Feb. 2014.

[7] F. Tan, M. K. Wu, M. Liu, M. Feng, and N. Holonyak, Jr., "Relative intensity noise in high speed microcavity laser," *Appl. Phys. Lett.*, vol. 103, no. 14, pp. 141116-1–141116-4, Oct. 2013.

[8] M. Liu, M.K. Wu, F. Tan, R. Bambery, M. Feng, and N. Holonyak, Jr., "780 nm oxide-confined VCSEL with 13.5 Gb/s error-free data transmission," *IEEE Photon. Technol. Lett.*, vol. 26, no. 7, pp. 702-705, Apr. 2014.

ACRONYMS

ICP: Inductively Coupled Plasma
RIE: Reactive-Ion Etch
DBR: Distributed Bragg Reflector
BCB: Benzocyclobuten